Journal of the Korea Institute of Applied Superconductivity and Cryogenics
Vol.5, No.1, (2003), pp.1~12

NMR/MRI Superconducting Magnet Technologies: Recent Activities at MIT Francis Bitter Magnet Laboratory

Yukikazu Iwasa and Haigun Lee

Francis Bitter Magnet Laboratory, Massachusetts Institute of Technology
CAMBRIDGE MA 02139 USA

Abstract– **In this paper we present a brief description and summary results of each of our recent activities in three areas, all devoted to NMR and MRI superconducting magnet technologies: 1) development of a high-field LTS / HTS NMR magnet; 2) development of a novel digital flux injector for *slightly* resistive NMR magnets; and 3) a proposal for a low-cost MRI magnet system based on MgB_2 composite and an innovative cryogenic design / operation concept.**

I. Introduction

The Magnet Technology Division of FBML has been playing a key role in the development of high-resolution superconducting MRI / NMR magnets. In the 1980s, FBML successfully built, and operated a 100 MHz /1200 mm MRI magnet for research use at FBML [1]. In the same period, a general method, currently widely used, for designing axial and radial shim coils for NMR and MRI magnets was developed [2,3]. The NMR magnets, designed, built, tested, and operated at FBML includes: 1) the *first* 300 MHz / 55 mm magnet wound with *multifilamentary* NbTi conductor, currently still in use for NMR research at FBML since 1978; 2) the *first* in the world 500 MHz / 55 mm magnet, operated continuously over a 15-year period, 1980-1995 [4]; 3) a 320 MHz / 104 mm magnet in operation for the past 22 years; and 4) a 600 MHz / 55 mm magnet [5], incorporating Nb_3Sn conductors and room-temperature ferromagnetic shimming in continuous operation at FBML since 1989. Presently, we are engaged in projects advancing NMR superconducting magnet technologies. These include: 1) a multi-year program to complete a high-resolution 1 GHz / 55 mm NMR magnet comprised of low- and high-temperature superconducting (LTS and HTS) coils–in Phase 1, we have successfully demonstrated the proof-of-concept of our design approach on an NMR magnet consisting of LTS and HTS coils by completing and operating the *first* LTS / HTS NMR magnet [6,7]; and 2) development of a novel flux pump ("digital flux injector") for NMR magnets that contain a slightly dissipative coil or coils, either LTS or HTS [8-10]. Other NMR magnet related superconducting magnet technologies developed at FBML include:

1. Use of "long" twist-pitch Nb_3Sn conductor to purposely trigger quench by means of filament-to-filament coupling AC losses generated by a fast field change [11].
2. Use of ferromagnetic shimming to achieve high-order field homogeneity [12].
3. Cryostat design for sub-4.2 K saturation operation that allows a continuous transfer of liquid helium for our 600 MHz / 55 mm system [5].
4. Graphite reinforcement of Nb_3Sn windings.
5. Development of superconducting splices between multifilamentary NbTi composites [13] and a technique to measure joint resistance as small as 0.1 picoΩ [14].
6. Development of superconducting splices between reacted multifilamentary Nb_3Sn composites and between reacted multifilamentary Nb_3Sn and multifilamentary Nb-Ti [12].

In this paper we present a description and summary results of each of our recent activities in three areas all devoted to NMR and MRI superconducting magnet technologies: 1) development of a LTS / HTS NMR magnet; 2) development of a novel digital flux injector for *slightly* resistive NMR magnets; and 3) a proposal for a low-cost MRI magnet system based on MgB_2 composite and an innovative cryogenic design / operation concept.

II. High-field NMR Magnets: 1 GHz (23.49 T) and Beyond

The recent progress in magnet technology has been impressive. The transition from Nb-Ti superconductor technology to the more difficult Nb_3Sn technology required almost 10 years. Today, low-temperature superconducting (LTS) magnet technology is enabling the development of the first 900 MHz (21.14 T) magnet systems [15, 16]. However, in fields above ~21 T the

current carrying capabilities of Nb_3Sn even at 1.8 K degrade so severely that ~21 T is generally considered the upper field limit for Nb_3Sn wires operated at 1.8 K. To achieve 1 GHz exclusively with LTS, development of advanced Nb_3Sn as well as Nb_3Al conductors is required. For example, the National Institute for Materials Sciences, Tsukuba Japan, is pursuing the development of

Nb_3Sn with Ti and Cu added to Sn and Nb_3Al as possible alternatives to Nb_3Sn for the 1 GHz magnet [17]. Even if these special conductors are to be successfully developed for the 1 GHz magnet, 1 GHz will be the practical upper limit for these advanced LTS. Sooner or later, for NMR magnets generating 1 GHz and *above*, high-temperature superconductors (HTS) must come into play. One important potential benefit of these advanced LTS materials is that these materials may within this decade enable an all-LTS 900 MHz NMR magnet to operate at 4.2 K.

We believe that for 1 GHz and above NMR magnets a combination of LTS coils and HTS coils, the so-called LTS / HTS configuration is more appropriate. In this configuration, LTS coils generate a central field up to 21.14 T (900 MHz) and an "HTS insert," a single or a set of coils, generates the balance. Thus in a 1 GHz (23.49 T) LTS/HTS magnet, such an HTS inserts generates a central field of 2.35 T. In a 1.1 GHz and 1.2 GHz magnets, the HTS insert contributions will be, respectively, 4.70 T and 7.05 T. The use of an HTS insert in the high-field region of a 1 GHz and above magnet offers the following advantages and potentials: 1) unlike an "LTS insert," wound with advanced versions of Nb_3Sn or Nb_3Al, which will undoubtedly be prone to premature quenches during the first few (or perhaps many) charging sequences, the HTS insert will operate quench-free the first time [18]; 2) an HTS has a potential to extend the upper NMR field to 35 T (~1.5 GHz) or even higher.

Phase 1 LTS / HTS NMR Magnet

In our first attempt to complete and demonstrate the proof-of-concept of the LTS / HTS magnet configuration, we recycled the LTS magnet from the 500-MHz all NbTi NMR magnet built at FBML in 1980 [4] as the LTS magnet of Phase 1 LTS / HTS NMR magnet. Figure 1 shows the cross section of the Phase 1 LTS / HTS magnet system with a room temperature bore of 55 mm; the support stand is not included in the drawing.

The main parameters of the Phase 1 background coil are listed in Table 1.

For the HTS Insert, a new mechanical support was designed and built that would provide the following capabilities:

- A precompression which is at least equal to the compressive force expected due to differential changes
  during cool down and coil energizing. For this insert the precompression load was calculated to be ~8,000 N.
- An axial displacement of up to ~3 mm, to allow the insert to align its field with that of the background coil.

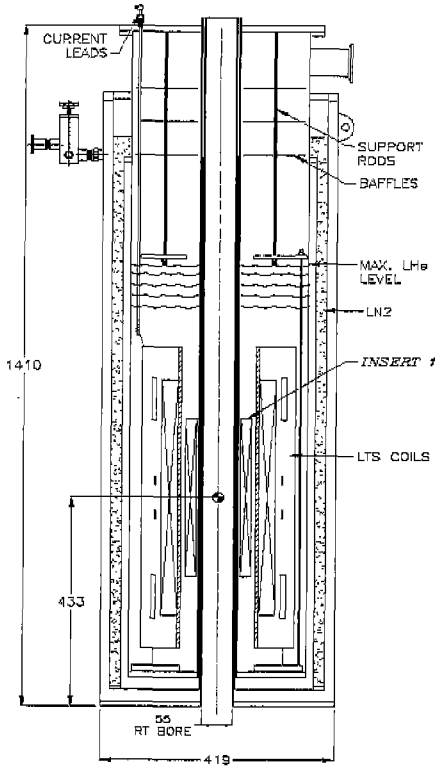

Fig. 1. Cross section of Phase 1 LTS / HTS NMR magnet system. Dimensions are in mm. Note the support stand is not included in the drawing [6].

TABLE I LTS Background coil parameters

Parameter	*Value*
Overall Winding Dimensions	
i.d.; [mm]	145.2
o.d [mm]	203
Length [mm]	488
Operating Conditions @ 4.2 K & I_{op} = 86 A	
$[\lambda J_{op}]coil$ [MA/m^2]	196.3
Central field @ I_{op} [T]	6.97

Table 2 shows basic parameters of the Phase 1 HTS Insert: 1) overall winding dimensions; 2) coil configuration in which the HTS insert is comprised of 50 double pancake (DP) coils; 3) parameters of high-strength 3-ply Bi-2223 /Ag tape used to wind each DP coil; 4) turn-to-turn
insulation dimensions; and 5) HTS insert operating conditions. Because the Insert is resistive due, as it has turned out, mostly to two HTS-HTS splices rather than index, it is operated, in driven mode. Figure 2 shows pictures of the Insert ready to be installed in the system cryostat.

Prior to the liquid helium test, the following tests were performed at 77 K on the HTS Insert:

TABLE II Parameters of Phase 1 HTS Insert

Parameter	*Value*
Overall Winding Dimensions	78.2; 120.3
i.d.; o.d [mm]	327.6
Length [mm]	
Configuration: 50-Double Pancake (DP) Magnet	0.178
Pancake-pancake space [mm]	72
Turns / pancake	44.8
Tape length / DP	1.12
Magnet inductance [H]	
HTS: High-Strength 3-Ply Bi-2223 / Ag	3.1; 0.25
Overall width; thickness [mm]	0.17
Bi-2223 /Ag thickness [mm]	1.63
HTS / Ag ratio	≥ 60
I_c @77 K, self field (straight sample) [A]	≥ 12
Index *n* @ 77 K, self field	
Turn-to-Turn Insulation: Nomex Paper	3.1; 0.038
Width; thickness [mm]	
Operating Conditions	4.2
Temperature [K]	49.0
Current (I_{op}) [A]	51.98
[λJ_{op}]*coil* [MA/m^2]	1.26
Central field @ I_{op} [T]	

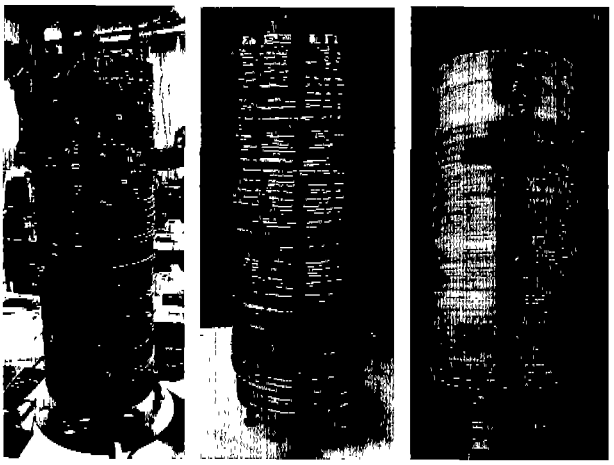

Fig. 2. HTS insert comprised of 50 double-pancake coils ready for installation into the Phase 1 system [7].

I_c Measurement Upon energizing, an I_c = 19.6 A was measured, which agrees well with a predicted value of I_c ≈ 20 A based on scaling ratios of the conductor.

Field Profile A search coil / integrator field probe was used to record the B_z field of the insert energized to 18 A. Agreement between experimental results and analysis was excellent.

Figure 3 shows a $B_z(z)$ plot for the Phase 1 LTS / HTS magnet at its design point at 4.2 K, generating a center field of 8.46 T corresponding to a proton frequency of 360 MHz. The LTS magnet was energized at 92.0 A and HTS Insert at 50.7 A. After reaching operating current the LTS magnet was placed in persistent mode while Insert was energized with a stable supply. Figure 4 shows an NMR signal at 350.321323 MHz captured with a 1 mm^3 sample.

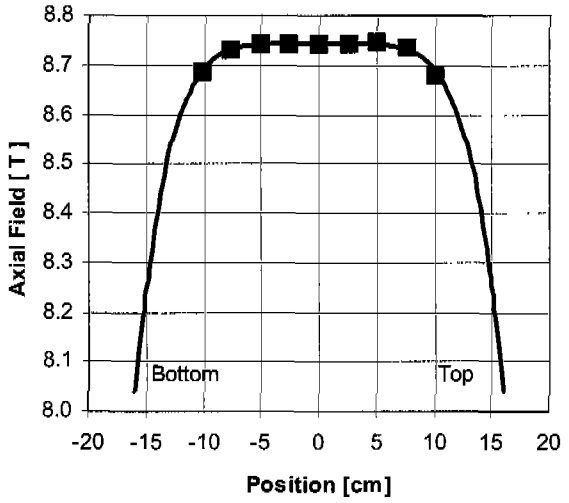

Fig. 3. Phase 1 LTS / HTS magnet $B_z(z)$ plot at 4.2 K. LTS magnet at 92.0 A and HTS insert at 50.7 A, measured (points) and computed (line) [6].

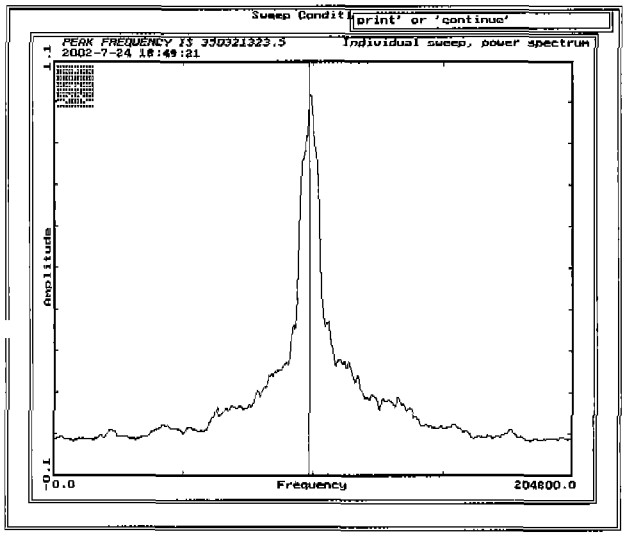

Fig. 4. NMR signal at 350.321323 MHz captured with a 1 mm^3 sample [6].

The Phase 1 LTS / HTS NMR magnet has successfully demonstrated of the proof of the concept that high-field, high-resolution NMR magnets may be constructed by combing an LTS magnet and an HTS insert. In the final 1 GHz system, the magnet will comprise of a 900 MHz LTS magnet (of a cold bore of at least 140 mm) and a 100 MHz HTS insert. We expect this insert to consist of double-pancake coils each wound with high-strength 3-ply Bi-2223 / Ag tape.

III. Digital Flux Injector

Flux pumps have been developed over the years primarily to induce a large current in a small-inductance superconducting load with a small current [19]. The primary goal is to reduce cryogenic heat load. In contrast to the "conventional flux pump," ours generates a current in the "microamperes" range [8] with a current in the amperes range. More importantly, the circuit and operational procedure of our flux pump is completely different from those of the original pumps [19]. Our pump represents an elegant option to achieve temporal field stability for an NMR magnet. Besides providing a low cryogenic load as compared with that of a driven system, our pump injects precisely metered quantities of flux and thus keeps the field within a narrow frequency band. Perhaps to distinguish it from the conventional flux pump, we call it a "digital flux injector".

General Description

Circuit Figure 5 shows the basic circuit of a *slightly resistive* insert coupled to a digital flux injector, comprised of the primary coil (self inductance L_p), secondary coil (L_s, M_{ps}) and switches (S_2, S_3) [8]. The insert, carrying operating current of I_{op}, is represented by self inductance (L_{mg}), and circuit resistance (R_{cir}).

The injector circuit contains three joints, J_2+, J_2–, and J_3. Joint J_3 involving an LTS-LTS splice, though it can be superconducting, needs to be only of a "small" resistance. J_2+ and J_2–, if the resistive magnet is of HTS, are HTS-LTS splices, which in the present state of technology will be resistive; however, their splice resistance only needs to be less than R_{cir}, not a difficult task. Diodes are generally connected for protection. In the prototype digital flux injector, they were not used because the system energy is low. Note that S_1 (with heater) represent a persistent mode switch for the insert; the switch requires Joints (J_1+, J_1–), which, for an HTS insert, are likely to remain resistive in the years to come.

Operation With S_2 and S_3 closed, I_p in the primary coil induces current I_s in the secondary coil such that $I_s > I_{opo}$,

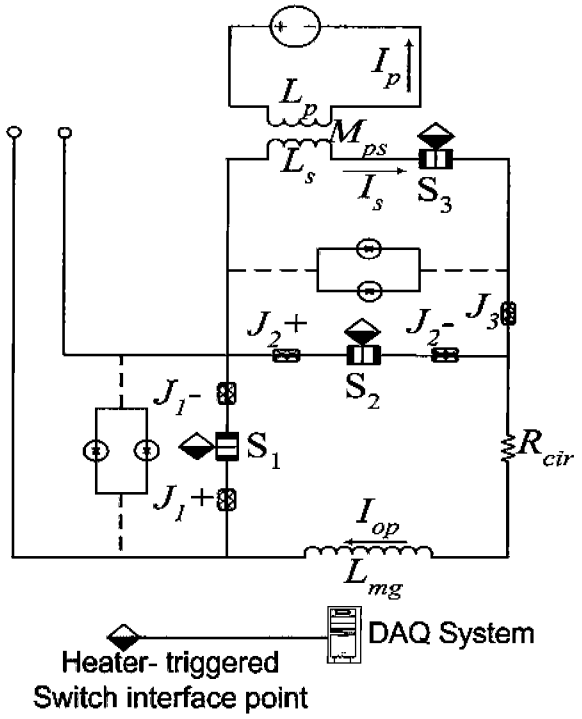

Fig. 5. Basic circuit of a *slightly resistive* insert coupled to a digital flux injector, comprised of the primary coil (self inductance L_p), secondary coil (L_s, M_{ps}) and switches (S_2, S_3) [8, 10].

where I_{opo} is the initial operating current of the insert. Note that I_{opo} is the current that must be kept within a range set by the system $\Delta f / f_o$ specification, where Δf and f_o are respectively, a specified frequency shift over a given time period and f_o is the system operating frequency. Upon opening of S_2, current commutation occurs between the insert circuit and the secondary circuit of the digital flux injector. The operational sequence is as follows.

1. For each flux injection cycle, S_2 and S_3 are closed and superconducting. The insert current, $I_{op} < I_{opo}$, flows through S_2.
2. I_p in the primary coil induces $I_s > I_{opo}$ in the secondary coil.
3. Switch S_2 is heated and becomes resistive. I_{op} in the insert and I_s in the secondary coil are forced to equilibrate, raising the insert current to I_{opo}.
4. S_2 is closed, shunting (isolating) the insert from the flux injector.
5. S_3 is opened and the secondary coil is discharged.
6. I_p is reduced to zero; S_3 is closed.

The cycle is complete. This cyclic action keeps I_{op} within $| \Delta I_{op} |$ of I_{opo}. Figure 6 shows schematic traces of I_{op} (t), I_s (t), and I_p (t) over one flux injection cycle time.

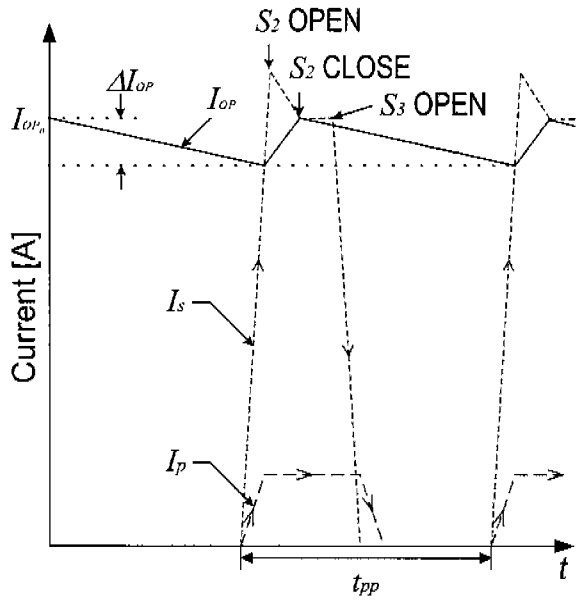

Fig. 6. Schematic traces of $I_{op}(t)$, $I_s(t)$, and $I_p(t)$ over one flux injection cycle time.

Flux Injector Configuration A digital flux injector for an NMR magnet must meet the following conditions and requirements: 1) the field generated by the primary and secondary coils of the injector over the uniform-field zone at the center of the NMR magnet must be zero, even though the flux injector would be located far away from the magnet center–this is achieved by assembling the injector coils as a toroid; 2) dissipation in the flux injector (coils and switches) must not be discharged directly into the liquid helium–this is achieved by placing the digital flux injector above the liquid level; the effluent vapor maintains the cold environment required by the injector; 3) I_s must be established in a time period much less than 10 s (a minimum practical for flux injection period; 4) opening time of each switch must be much less than a flux injection period–not a difficult requirement to meet with a digital flux injector stationed in the vapor environment.

Prototype Digital Flux Injector

Table 3 presents parameters of the primary and secondary coils of the prototype digital flux injector [9]. As noted above, both primary and secondary coils are toroids. The Nb_3Sn insulated tape of General Electric (GE) is used for the superconducting parts of the flux injector, i.e., the primary and secondary coils; switches S_2 and S_3; and connections, which are spliced only at joint J_3, a simple Pb-Sn soldered tape-tape overlap. Figure 7 shows a photograph of the prototype digital flux injector and the second load magnet (L_{mg} = 2.65 H) used in the experiment [10]. Note that the transformer coils are placed between

TABLE III Prototype Digital Flux Injector [9]

Parameter	*Primary*	*Secondary*
Toroid (100 mmϕ): 4 Double Pancakes (DP)	40.0; 67.8	36.8; 38.2
DP i.d.; o.d. [mm]	7.2	6.5
Width [mm]	84	4
# turns / DP		
L (measured) [μH]	2,130	16
M_{ps} [μH]	73	73
Conductor: GE Nb_3Sn Tape (3.1 mm × 0.4 mm]		
Length / DP [m]	14.2	0.5

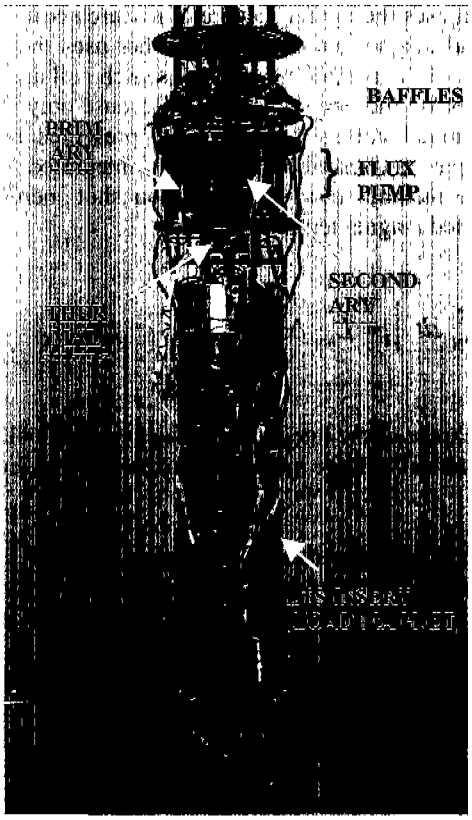

Fig. 7. Photograph of the prototype digital flux injector and the second load magnet (L_{mg} = 2.65 H) used in the experiment [10].

two plates; each of 6.35-mm thick copper and acts as a temperature stabilizer for the coils. Switches S_2 and S_3 are placed directly beneath the bottom copper plate but above the liquid helium level to keep switching dissipation from directly depositing heat in the bath; they are quite different in construction from usual persistent

switches, such as S_1 installed in the load magnet. Switches S_2 and S_3 must turn on and off with a short time constant; these thermally activated switches are designed to have a minimum thermal inertia for rapid (in seconds) temperature change, but a normal-state resistance sufficient for switching. The current-carrying element of each switch is the same GE tape used for the transformer coils. Each switch is comprised of two turns of the GE tape wound over a 50-mmϕ bobbin made of a thin stainless steel shim stock. For proper thermal isolation and mechanical integrity, a layer of Stycast 2850FT epoxy was applied to the outer layer of each switch [9].

Measurement Techniques Two independent but complementary methods may be used to quantify flux increments injected into the Nb-Ti load magnet [8]. One method uses the output voltage of a search coil placed in the load magnet bore, while the other uses the terminal voltage of the magnet itself. Both search coil and magnet voltages are then time integrated. Because only results of the terminal voltage technique are presented here, this technique is described. For the integrated terminal voltage method, each flux injection shot increases the integrated magnet terminal voltage:

$$\left[\int V_{mg}^{\uparrow} \, dt \right]_1 = L_{mg} \Delta I_{op} \quad (1)$$

Thus a trace of the integrated voltage vs. time will consist of a series of voltage increments, each given by Eq. 1.

Results and Discussion Figure 8 shows a set of voltages and currents vs. time plots corresponding to the first 15 shots of an injection sequence with a cyclic period of 10 s and I_s = 0.363 A. The top traces are the terminal voltage (spikes; left scale) and ΔI_{op} (dashed; right scale). The bottom trace is the current I_s through the primary coil. Large spikes are induced in the terminal voltage every time Switch S_2 is opened to induce a current increment ΔI_{op} in the magnet circuit. Each current increment is 8 μA, with a cumulative increase of 120 μA after 15 consecutive shots. Analyzing the circuit (Fig. 5) for ΔI_{op}, we obtain an expression for ΔI_{op} [8]

$$|\Delta I_{op}| = \frac{L_s (I_s - I_{op})}{L_{mg} + L_s} = \frac{M_{ps} I_p - L_s I_{op}}{L_{mg} + L_s} \quad (2)$$

Inserting other terms (M_{ps} = 73 μH, I_{op} = 0, L_s = 16 μH) into Eq. 2, we obtain ΔI_{op} = 9.96 μA, which agrees reasonably well with 8 μA measured. The agreement was also good with the first load magnet (L_{mg} = 9.6 H) [9].

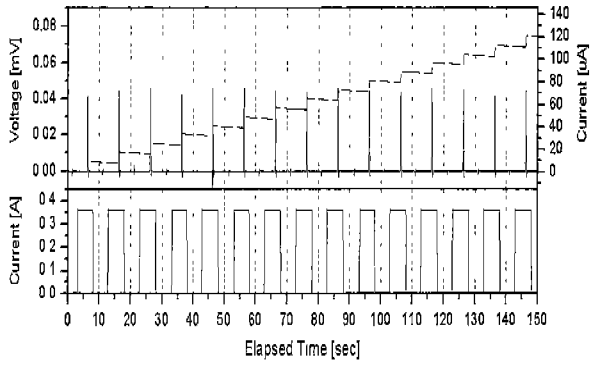

Fig. 8. Set of voltages and currents vs. time plots corresponding to the first 15 shots of an injection sequence with a cyclic period of 10 s and I_s = 0.363 A. Top: Terminal voltage (spikes; left scale) and ΔI_{op} (dashed; right scale); bottom): current *Is* through the primary coil.

Full-Scale Digital Flux Injector

Operation of this digital flux injector with two magnet loads has demonstrated that each flux injection shot can add a metered amount of flux into a magnet load, in excellent agreement with analysis. A full-scale digital flux injector has been proposed for the HTS Insert of the Phase 1 350MHz LTS / HTS NMR magnet described above. Because of a circuit resistance in the HTS Insert, the LTS / HTS magnet by itself cannot be operated in persistent mode; the injector enables it effectively.

IV. Low-Cost HTS MRI Magnet System

As an economically viable, i.e., low-cost, MRI magnet system based on HTS, we have been studying the feasibility and practically of a low-cost, i.e., commercially viable, superconducting MRI magnet system specifically targeted for use in small hospitals, rural communities, and underdeveloped nations. The MRI system incorporates MgB_2 composite conductor and an innovative cryogenic design / operation concept.

Magnesium Diboride (MgB_2)

For use in small hospitals, rural communities, and underdeveloped nations, our choice for a superconducting MRI magnet would be a high-temperature superconductor (HTS) rather than a low-temperature superconductor (LTS), simply because the cooling source for such an HTS magnet can easily be

provided by a cryocooler, which comes as an integral part of the system. (To maintain the magnetic field even during a brief period of occasional power outages, an innovative cryogenic design /operation concept, described briefly below, is introduced to this basic HTS system). With an NbTi-based MRI magnet, which has to guard against the same failure mode, its cooling source must be liquid helium. It should be noted that among commodities, liquid helium is one of the least accessible, even in the developed nations let alone in the regions the proposed system is targeted for. If not with MgB_2 magnets, however, it is not possible for an HTS-based MRI magnet to meet the most important requirement for commercially viability: low cost. Critical current densities of MgB_2 clearly makes this superconductor a viable conductor option for magnets generating up to 5 T and operating in the same operating temperature range 10-15 K as in our proposed system. Indeed, this requirement of low cost is the chief reason for selecting 0.5 T for a center field of a commercial low-cost 0.5 T whole-body MRI systems. Also to satisfy this low-cost criterion, the MRI magnet would not be actively shielded as are most standard 1-1.5 T MRI systems marketed nowadays.

As noted above, for low-field applications MgB_2 satisfies the low-cost requirement: its cost is projected by the end of 2004 to be even less than NbTi, at the moment the least expensive superconductor available and suitable for magnets such as low-field MRI systems. A clear-cut advantage of MgB_2 over NbTi is its zero-field critical temperature, 39 K vs. 9.8 K, enabling it to operate in the range 10-15 K even in a field of 5 T. Thus our choice of MgB_2 for low-cost MRI magnets is based on two key points: 1) its cost near term (end of 2004) is projected to be comparable to and potentially even less than NbTi; 2) its proposed operating temperature range of 10-15 K permits adaptation of the innovative design / operation concept that is particularly suitable for use in the regions where liquid cryogens are among least accessible commodities and where electric power supplies are not reliable.

Innovative Design / Operation Concept

The innovative cryogenic design / operation concept, developed at FBML [20-24], introduces a volume of solid cryogen, nitrogen in the proposed system, in the "cold body" housing the magnet, thereby enhancing significantly the cold body's heat capacity. The solid nitrogen enhanced enthalpy of the magnet body permits operational options that are not possible with a magnet cooled simply by a cryocooler. One option, adopted in the proposed system, is to operate the magnet at a nominal temperature, e.g., 10 K, with the cryocooler continuously running. The solid nitrogen in the magnet housing would enable the magnet to maintain its field over a time period, e.g., 1 day, even when electricity is cut off from the cryocooler by a power outage or system malfunction, in which case the cryocooler would be automatically thermally decoupled from the magnet housing. In this system, the magnet is designed to maintain its nominal operating field of 0.5 T up to 15 K, which is reached during a 1-day electricity failure. At 15 K, the magnet is recooled to and operated at 10 K, ready for the next power outage.

"Dry" Cryocooler / MRI Magnet

General Electric (GE) initiated a trend towards "dry" (no liquid cryogen) superconducting MRI magnets in the early 1990s by introducing an all-Nb_3Sn magnet / cryocooler MRI system. The magnet operated at 10 K, the practical upper temperature with Nb_3Sn. Despite the popularity of its dry magnet, because of its high cost compared with that of a "wet" (liquid helium cooled) NbTi system, due largely to the high cost of Nb_3Sn, the dry 10-K Nb_3Sn magnet could not compete against the wet 4.2-K NbTi magnet. Clearly, the key to market penetration for dry MRI systems is an HTS that in cost and performance can excel NbTi. We believe such an HTS is Magnesium Diboride (MgB_2), discovered in January, 2001. Figure 9 presents field vs. temperature plots of MgB_2 and two staples of superconductor for magnets, NbTi and Nb_3Sn [25]. The MgB_2 plot makes it clear that the applicable field range of MgB_2 extends into the 10-30 K range impossible with NbTi and Nb_3Sn. As shown in Fig. 10 [26], its critical current density in the temperature range 10-15 K in low fields is well above the minimum level to formulate MgB_2 into a "composite" conductor that must include not only MgB_2 but also normal metals to make the composite meet strength, stability, and protection requirements of a working magnet. As early as 2002, *only one year after discovery*, it was agreed in the superconductivity community that cost of MgB_2 would easily match that of NbTi. That is, this combination of MgB_2 and an innovative cryogenic concept enables the proposed MRI magnet system to perform even under conditions less reliable than those tacitly assumed in standard MRI magnet systems.

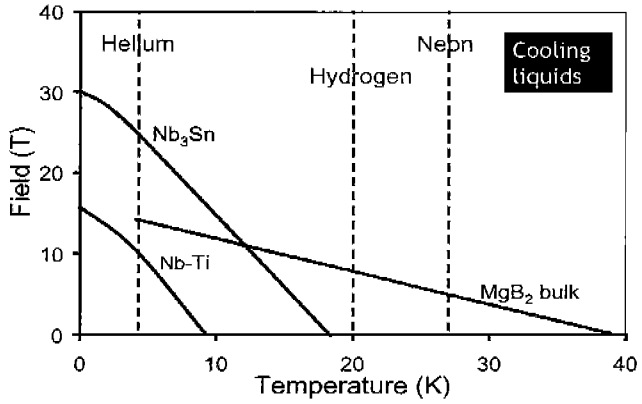

Fig. 9. Field vs. Temperature plots of MgB_2 bulk and two staples of superconductor for magnets, NbTi and Nb_3Sn. Boiling temperatures of helium, hydrogen and neon are shown by the vertical dashed lines [25].

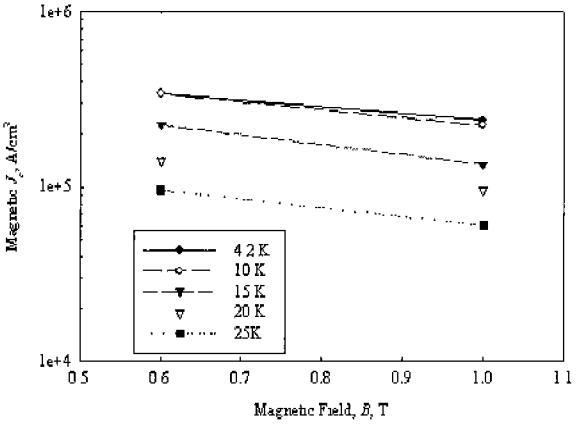

Fig. 10. MgB_2 critical current density in the temperature range 10-15 K in low [26].

Reference Design for Low-Cost 0.5 T / 80 cm MRI Magnet

Table 4 shows coil parameters of a first-cut reference design for a low-cost 0.5 T / 80 cm whole-body MRI magnet to be wound essentially with reacted MgB_2 composite and equipped with the same innovative cryogenics system. The magnet operates at 98.6 A and stores a total magnetic energy of 177 kJ. Note that a B_{pk} = 1.53 T occurs in Coils 1 and 3, both correction coils, each placed, respectively, in the left- and right-hand sides of the magnet center. A maximum stress of 69 MPa, occurring at the end coils, is still a level considered quite benign. The magnet's computed field homogeneity is 1.084 ppm over a 25 DSV. With cold shim coils this can be improved to 0.1 ppm; ferromagnetic shimming will further improve it to 0.01 ppm.

TABLE IV Coil Parameters of 0.5 T / 80 cm MRI Magnet
(Wire: D_{bare} = 1.0 mm; $D_{overall}$ = 1.076 mm; I_{op} = 98.55 A; E_{total} = 177 kJ; L = 36.4 H)

Coil	i.d. [mm]	o.d. [mm]	width [mm]	corner* [mm]	volume [cm³]	# layers	turns	B_{pk} [T]	σ [MPa]	length [km]
1	884.4	925.7	132.3	-654.7	7,770	22	2706	1.53	69.2	7.7
2	860.0	867.7	893.0	-446.5	9,380	4	3320	0.52	27.7	9.0
3	884.4	925.7	132.3	+522.4	7,770	22	2706	1.53	69.2	7.0

* Position of the left-hand side of coil end measured in the magnet axis direction with the coil center designated at z=0.

Magnet Design and Operation Issues

Here, we discuss key magnet design and operational issues: stability; protection; electromagnetic stresses; persistent mode operation; persistent switch; thermal expansion in the 10-15 K range. The cryogenics is discussed separately.

Stability The demonstration magnet operates nominally at 10 K and to 15 K during a period of up to 1 day when its cryocooler is shut off. In the maximum field of ~1 T and carrying a current of ~100 A, the conductor will have a current-sharing temperature of ~20 K. We may thus regard this magnet, as noted earlier, to be *absolutely* stable against those disturbances that occur within the winding and can cause instability in high-performance ("adiabatic") NbTi and Nb_3Sn magnets operating at 4.2 K [18]. Note that the heat capacities of winding materials increase enormously from those at 4.2 K in the temperature range 15-20 K, i.e., ~30 times (15 K) and ~80 times (20 K).

Protection Because the magnet operates in persistent mode, shunted with a persistent switch, the voltage across the entire magnet will remain zero even if a small section of the winding is driven normal, which as noted above, an event extremely unlikely to occur in this magnet. A standard protection approach for an "isolated" magnet operating in persistent mode is to divide the winding into several subsections, each shunted by a combination of a resistor and diodes [18]. In the event of a local quench, this subdivision enables current to be induced through each loop comprised of a shunt resistor and its subsection, causing dissipation in the resistor, thereby preventing dissipation in one localized region of the winding.

The shunt resistors and diodes will be placed in a vacuum space outside of the magnet housing, thermally anchored to the cold radiation shield. Although this is unlikely, the worst scenario is for the entire magnetic energy (~72 kJ) in the magnet to be dissipated in the shunt resistors. To limit the maximum temperature in the shunt resistors in this event to be less than room temperature, the total mass of the shunt resistors must be ~1 kg. Resistor

values, each in the range of ~0.5-1 Ω, will be determined during the design phase.

Electromagnetic Stresses Electromagnetic stresses do not pose any undue problem in this full-scale MRI magnet, because field levels in the coils are no greater than ~2 T. Note that the maximum stress is only 69 MPa (Table 4).

Persistent Mode Operation–Sources of Resistance: Splice & Index The proposed magnet operates in persistent mode. This implies that the total magnet circuit resistance must be *small*. Specifically, for this magnet, with a self inductance of 36.4 H, to satisfy a temporal stability specification of 0.01 ppm /h, the total resistance must not exceed 102 picoΩ. Here we shall briefly discuss the two sources of resistance–splices and index–that must be minimized or ideally eliminated, in a persistent-mode superconducting magnet.

Splice With as many as ~20 MgB_2-MgB_2 splices in the magnet, each splice resistance must not exceed ~5 picoΩ, a level no more demanding than that imposed for splices among LTS. It is expected that this level of splice resistance can be met with MgB_2 composite, which is much closer to Nb_3Sn composite than its cousins BSCCO and YBCO, both ceramics.

Index Perhaps because MgB_2 is a compound like Nb_3Sn (intermetallic compound) rather than a ceramic like BSCCO and YBCO, its index (n value) could be expected to be inherently better than those typical for Bi-2223 /Ag, i.e. 15-20. This statement is supported by the latest and extensive review article on MgB_2 by Flukiger, et al. [27]. The article reports that n for "well-packed" (small porosity) MgB_2 ranges 70-100, a range even greater than Nb_3Sn (30-50), in the field range 4-5 T, decreasing with field. Because the maximum field in the demonstration magnet and a full-scale 0.5 T MRI magnet is below 2 T, we expect index to pose no serious problems for persistent mode operation of this full-scale MRI magnet. Also to be noted is that the operating current I_{op} of these magnets is ~100 A, a fraction of an expected critical current I_c of the magnet conductor, thus reducing effective index resistance further because the index resistance is proportional to $(I_{op}/I_c)^n$ [18].

Persistent Switch The demonstration magnet must be terminated with a persistent switch wound with unreacted MgB_2 wire with a "small" amount of or no copper in the matrix. This is to maintain a reasonable normal-state resistance during the charging mode. For this magnet with a self inductance of 36.4 H, a supply voltage across the magnet of 0.5 V will require ~2 h to charge the magnet to ~100 A. At this charging voltage a normal-state switch resistance of 0.5 Ω will draw a current of 1 A. dissipating 0.5 W, a level clearly manageable by the cryocooler 2nd stage. Although the 2nd stage can generally manage this extra heating that occurs only during the charge-up sequence, it is important to keep this heating level below 1 W. This is, as discussed below, because ΔT across the thermal switch connecting the 2nd stage cold head and the magnet housing must be kept no greater than 0.5 K.

Thermal Expansion (10-15 K) The coefficient of linear thermal expansion, $\alpha(T)$, is defined by:

$$\alpha(T) = \frac{1}{L_o}\left(\frac{\partial L}{\partial T}\right)_P \tag{3}$$

where L_0 is the initial length. The subscript P implies a constant pressure process. $\alpha(T)$ varies with T as does specific heat, as:

$$\alpha(T) = aT + bT^3 \tag{4}$$

Based on an experimental $\alpha(T)$ plot of copper [28] in the range $0 \le T \le 50$ K, we find for copper: $a_{cu} = 5 \times 10^{-9}$ K^{-2} and $b_{cu} = 3 \times 10^{-11}$ K^{-4}. For $\Delta T_{op} = 5$ K, between 10 K and 15 K, we may compute $\Delta L/L_o$ for copper, $(\Delta L/L_o)_{cu}$, by integrating Eq. 3 between 10 K and 15 K. Here copper is selected as a representative material for the winding materials. Because copper is a pure metal, $(\Delta L/L_o)_{cu}$ over this temperature range is likely to be considerably greater than corresponding values for winding materials. Thus:

$$\left(\frac{\Delta L}{L_o}\right)_{cu} = \int_{10K}^{15K}\left(5\times10^{-9}T + 3\times10^{-11}T^3\right)dT = 0.62\times10^{-6} \tag{5}$$

This *linear* change obviously takes place in three dimensions. Because the magnet is symmetric in all three axes (z, r, ϕ), a linear change of 0.62 ppm does not translate directly to a spatial field inhomogeneity of 0.62 ppm; its impact should be far less and not be a concern.

Cryogenic Issues

Important cryogenic issues for the proposed system are: 1) cryocooler; 2) thermal switch; 3) dissipation within and heat transfer to the cold body; 4) warm-up and

recooling processes; and 5) nitrogen safety. Each is discussed below.

Cryocooler
A cryocooler for this proposed system will have cooling capacities typically of: (1st stage) 35 W @45 K; (2nd stage) 6 W @10 K.

Thermal Switch
One key feature of this proposed system is to thermally disconnect the cryocooler when its electricity supply is cut off upon a power outage. During this power outage, which for this MRI magnet is assumed to last 1 day, the cold body warms up, reaching the maximum allowed operating temperature of 15 K after 1 day. To minimize heat input from the 2nd stage cold head to the cold body and that from the 1st stage to the cold radiation shield, a thermal switch will be installed between each thermal path.

The basic design of the on /off part of a thermal switch is a "multi-lam," a commercially available copper plug / socket connector used primarily for electrical applications. For thermal applications requiring a small level of ΔT across the switch, i.e., < 0.5 K, modifications are necessary. For example, Be-Cu fins (for elasticity) of multi-lams, may need to be substituted with thermally conductive metal.

Heat Generated Within and Heat Transfer to Cold Body
When the cold body (magnet housing) is thermally decoupled from the cryocooler, it begins to warm up, from its initial temperature of 10 K. Here, we examine heat generated within and that transferred to the magnet housing during a warm-up sequence.

Generation Within Cold Body There are three principal sources of dissipation within the cold body, all in the magnet. They are: 1) AC losses; 2) splices; and 3) index. Under the persistent mode operation condition assumed for this system, AC losses will be absent. Also, because in order to satisfy temporal stability of the proposed demonstration magnet, i.e., 0.01 ppm / h, which translates to a maximum total circuit resistance, splices and index, of ~100 picoΩ, this resistance, even if it were indeed present, generates a dissipation rate of 1 μW, a level completely negligible for this system. Thus, it is safe to state that the electromagnetic dissipation within this magnet housing may be neglected altogether.

Heat Transfer To Cold Body To quantitatively estimate total heat transferred to the magnet housing during the warm-up period, three sources of heat transfer to the cold body–radiation, convection, conduction–must be considered. Generally, it is quite difficult to accurately estimate each term for a "working" system with many components even if its general shape is cylindrically symmetric. Fortunately, we have built, operated, and measured the thermal performance of a system, though much smaller in dimensions, that is essentially similar to the proposed system [21-24]. One major difference between the previous and present systems is the temperature of the warm environment that surrounds each cold body: in the previous system, it was room temperature, while for the present system it is cold, ranging from 45 K initially to 120 K. An estimated total average heat input to the magnet housing of this demonstration system, while it is decoupled from the 2nd stage of the cryocooler, is 100 mW

V. Conclusions

We have presented a brief description and recent results from each of three current activities all devoted to advance superconducting NMR and MRI magnet technologies. The Phase 1 LTS / HTS NMR magnet project has successfully demonstrated the proof-of-concept for a high-field (1 GHz and beyond), high-resolution magnet configuration comprised of LTS background-field magnet and an HTS insert. In our program we chose to assemble the HTS insert with double-pancake coils wound with high-strength Bi-2223 / Ag tape. The digital flux injector has successfully been demonstrated to be a viable device that enables a slightly resistive NMR magnet operated effectively in persistent mode because the digital flux injector can inject a precisely metered amount of flux in such a magnet. We are confident that the proposed MRI magnet system based on MgB_2 and an innovative cryogenic design / operation concept should lead to a viable (const competitive) and reliability-enhanced commercial low-field MRI particularly suitable in use small hospital, rural communities, and underdeveloped nations.

Acknowledgement

We thank Juan Bascunan and Emanuel Bobrov for their contribution in the three programs described in this paper. We also thank Sang Kwon Jeong and Homin Kim for their participation in the digital flux injector program during their stay at FBML as visiting scientists.

References

[1] J.E.C. Williams, E.S. Bobrov, W.F.B. Punchard, R.D. Pillsbury et al., NMR Magnet for Imaging, *Journal De Physique*, **45**(1), 691 (1984).

[2] E.S. Bobrov, W.F.B. Punchard, A general Method of Design of Axial and Radial Shim Coils for NMR and MRI Magnets, *IEEE Transactions on Magnetics*, **24**(1), 533 (1988).

[3] E.S. Bobrov, J.E.C. Williams, R.D. Pillsbury, Jr., W.F.B. Punchard, R.E. Schwall, H.R. Segal, and L.J. Neuringer, "A 60 cm Bore 2.0 Tesla High Homogeneity Superconducting Magnet for Magnetic Resonance Imaging," *IEEE Transactions on Magnetics*, **23**(2), 1303 (1987).

[4] J.E.C. Williams, L.J. Neuringer, E.S. Bobrov, R.J. Weggel, D. Ruben, and W. Harrison, "Magnet system of a 500 MHz NMR Spectrometer. Part I: Magnet Development," *Rev. Sci. Inst.* **52**, 649 (1981).

[5] J.E.C. Williams, S. Pourrahimi, Y. Iwasa, and L.J. Neuringer, "600 MHz Spectrometer Magnet," *IEEE Trans. Mag.* **25**, 1767 (1989).

[6] J. Bascunán, H. Lee, E.S. Bobrov, and Y. Iwasa, "A low– and high-temperature superconducting (LTS/HTS) NMR magnet: design and performance," (presented at the ASC2002, Houston, August 2002) *IEEE Trans. Appl. Superconduc.* (2003).

[7] Haigun Lee, Juan Bascunán, Yukikazu Iwasa, "A high-temperature superconducting double-pancake insert for an NMR magnet" (presented at the ASC2002, Houston, August 2002), *IEEE Trans. Appl. Superconduc.* (2003).

[8] Yukikazu Iwasa, "Microampere flux pumps for superconducting NMR magnets Part 1: Basic concept and microtesla flux measurement," *Cryogenics* **41**, 384 (2001).

[9] S. Jeong, H. Lee, and Y. Iwasa, "Superconducting flux pump for high-temperature superconducting insert coils of NMR magnets," Presented at the Cryogenic Engineering Conf. (Madison, WI, July 2001), *Adv. Cryogenic Engr.* (2002).

[10] Haigun Lee, Ho-Min Kim, Yukikazu Iwasa, "A flux pump for an NMR magnet,"(presented at the ASC2002, Houston, August 2002), *IEEE Trans. Appl. Superconduc.* (2003).

[11] Mamoon I. Yunus, Yukikazu Iwasa, and John E.C. Williams, "AC loss induced quenching in multicoil adiabatic superconducting magnets," *Cryogenics* **35**, 93 (1995).

[12] J.E.C. Williams, E.S. Bobrov, Y. Iwasa, W.B.F. Punchard, J. Wrenn, and A. Zhukovsky, "NMR magnet technology at MIT," *IEEE Trans. Mag.* **28**, 627 (1992).

[13] M.J. Leupold and Y. Iwasa, "Superconducting joint between multifilamentary wires (Part I)–Joint-making and joint results," *Cryogenics* **16**, 215 (1976).

[14] Y. Iwasa, "Superconducting joint between multifilamentary wires (Part II) – Joint evaluation technique," *Cryogenics* **16**, 217 (1976).

[15] Alan Street, "Superconducting magnets get bigger and better," *The Industrial Physicist* October/November 2002, pp 32-38.

[16] T. Kiyoshi, A. Sato, T. Takeuchi, K. Itoh, S. Matsumoto, O. Ozaki, K. Fukushima, H. Wada, M. Yoshikawa, T. Kamikado, S. Itoh, T. Miki, T. Hase, M. Hamada, Y. Kawate, and R. Hirose, "Persistent-mode operation of a 920 MHz high-resolution NMR magnet," *IEEE Trans. Appl. Superconduc.* **12**, 711 (2002).

[17] See, for example, Y. Iijima, A. Kikuchi, N. Banno, T. Takeuchi, K. Inoue, "Direct formation of A15 phase through RHQ treatment in RIT-processed Nb / Al-Cu precursor wire," (presented at the ASC2002, Houston, August 2002) *IEEE Trans. Appl. Superconduc.* (2003).

[18] Yukikazu Iwasa, *Case Studies in Super conducting Magnets* (Plenum Press, New York, 1994).

[19] Martin N. Wilson, *Superconducting Magnets* (Oxford University Press, New York, 1983).

[20] Yukikazu Iwasa, "A 'permanent' HTS magnet system: key design & operational issues," in Advances in Superconductivity X [Proc. 10th International Sympo. Superconductivity (ISS'97), (Springer-Verlag, Tokyo, 1998).

[21] Benjamin Haid, Haigun Lee, Yukikazu Iwasa, Sang-Soo Oh, Hong-Soo Ha, Young-Kil Kwon, Kang-Sik Ryu, "Stand-alone solid nitrogen cooled 'permanent' high-temperature superconducting magnet system," IEEE Trans. Appl. Superconduc. **11**, 2244 (2001).

[22] Benjamin J. Haid, "A 'permanent' high-temperature superconducting magnet operated in thermal communication with a mass of solid nitrogen," *Ph.D. thesis*, Dept. of Mechanical Engineering, Massachusetts Institute of Technology, Cambridge (June, 2001).

[23] Benjamin J. Haid, Haigun Lee, Yukikazu Iwasa, Sang-Soo Oh, Young-Kil Kwon, and Kang-Sik Ryu, "A 'permanent' high-temperature superconducting magnet operated in thermal communication with a mass of solid nitrogen," Cryogenics **42**, 229 (2002).

[24] Benjamin J. Haid, Haigun Lee, Yukikazu Iwasa, Sang-Soo Oh, Young-Kil Kwon, and Kang-Sik Ryu, "Design analysis of a solid heat capacitor cooled 'Permanent' high-temperature superconducting magnet system," Cryogenics **42**, 617 (2002).

[25] David C Larbalestier, "MgB_2–A large scale applications perspective," [APS March meeting MgB_2 Press Brief, March 12, 2001].

[26] Mike Tomsic of Hyper Tech Research Inc. (private communication, March 2003).

[27] R. Flukiger, H. L. Suo, N. Musolino, C. Beneduce, P. Toulemonde, P. Lezza, "Superconducting properties of MgB_2 tapes and wires,'' Physica C Vol. 385, 286 (2003).

[28] *Materials at Low Temperatures*, Eds. Richard P. Reed and Alan F. Clark (American Society for Metals, 1983)